Journal of Medicinal Chemistry

pubs.acs.org/jmc

Article

Optimization of the Prodrug Moiety of Remdesivir to Improve Lung Exposure/Selectivity and Enhance Anti-SARS-CoV-2 Activity

Hongxiang Hu, Mohamed Dit Mady Traore, Ruiting Li, Hebao Yuan, Miao He, Bo Wen, Wei Gao, Colleen B. Jonsson, Elizabeth A. Fitzpatrick, and Duxin Sun*

Cite This: https://doi.org/10.1021/acs.jmedchem.2c00758

Read Online

ACCESS | Metrics & More | Article Recommendations | Supporting Information

ABSTRACT: COVID-19 patients with severe symptoms still lack antiviral treatment options. Although remdesivir is the only FDA-approved drug for those patients, its efficacy is limited by premature hydrolysis to nucleoside (NUC), low accumulation in the disease-targeted tissue (lungs), and low antiviral potency. In this study, we synthesized a new series of remdesivir analogues by modifying the ProTide moiety. In comparison with remdesivir, the lead compound MMT5-14 showed 2- to 7-fold higher antiviral activity in four variants of SARS-CoV-2. By reducing premature hydrolysis in hamsters, MMT5-14 increased the prodrug concentration by 200- to 300-fold in the plasma and lungs but also enhanced lung accumulation of the active metabolite triphosphate nucleosides (NTP) by 5-fold. Compared to remdesivir, MMT5-14 also increased the intracellular uptake and activation in lung epithelial cells by 4- to 25-fold. These data suggest that MMT5-14 could be a potential antiviral drug to treat COVID-19 patients with severe symptoms.

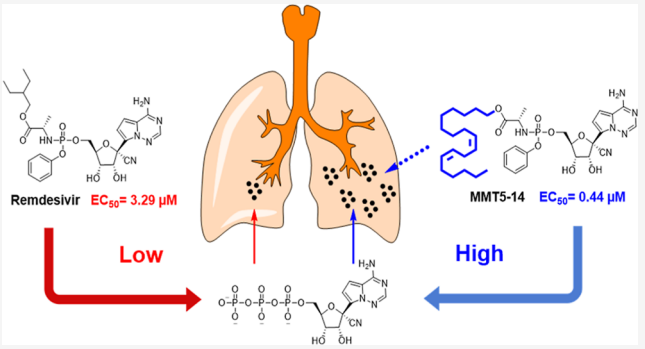

INTRODUCTION

Global pandemic coronavirus disease 2019 (COVID-19), caused by severe acute respiratory syndrome coronavirus 2 (SARS-CoV-2), has infected more than 500 million people and caused 6 million deaths worldwide as of May 2022 according to the WHO report (https://covid19.who.int/). Despite the recent successful development of antiviral drugs for treating mild and moderate COVID-19,[1,2] COVID-19 patients with severe symptoms still lack effective antiviral treatment options. Remdesivir (VEKLURY), approved by the FDA in October 2020, was the only antiviral drug in COVID-19 patients with severe symptoms.[3,4] The approval of remdesivir was based on the clinical study ACTT-1 (NCT 04280705), in which subjects with moderate or severe symptoms showed shorter recovery time (median 10 days vs 15 days in the placebo group, the 95% CI of recovery rate ratio is 1.12−1.49), higher odd ratios of improvement at day 15 (the 95% CI of odds ratio in the eight-point ordinal scale is 1.25−1.91), and lower mortality at day 29 (11% vs 15% in the placebo group).[5] The combination of remdesivir with other clinical interventions, such as immune modulators (e.g., baricitinib or tocilizumab), supplemental oxygen, or SARS-CoV-2-targeting monoclonal antibodies (e.g., casirivimab, imdevimab, or sotrovimab), has improved the clinical outcome of COVID-19 patients by reducing the fatality rate.[6,7] However, several other clinical trials using remdesivir against SARS-CoV-2, as reported in the WHO solidarity trial,[8] GS-US-540-5773 (NCT04292899),[9] and GS-US-540-5774 (NCT04292730),[10] failed to show any statistical difference between the remdesivir treatment group and the control group when considering the odd ratios of improvement in clinical status (NCT04292730, 10 day administration)[10] or mortality rate (solidarity trial, 95% CI is 0.81−1.11).[8]

Remdesivir was designed as a prodrug of nucleoside monophosphate (NMP) using the ProTide strategy, which generates active metabolite nucleoside triphosphate (NTP) to inhibit its target RNA-dependent RNA polymerase (RdRp).[11,12] The prodrug remdesivir was designed to enhance the cell permeability of NMP and to overcome the rate-limiting first step phosphorylation of the nucleoside (NUC) inside cells. Ideally, the intact prodrug remdesivir enters the cells and then is cleaved by intracellular carboxylesterase 1 (CES 1) and phosphoramidases (HINT1-3) to generate NMP that is subsequently phosphorylated to NTP for its antiviral activity.

Three shortcomings of remdesivir may have contributed to its limited clinical efficacy: (1) premature hydrolysis of

Received: May 13, 2022

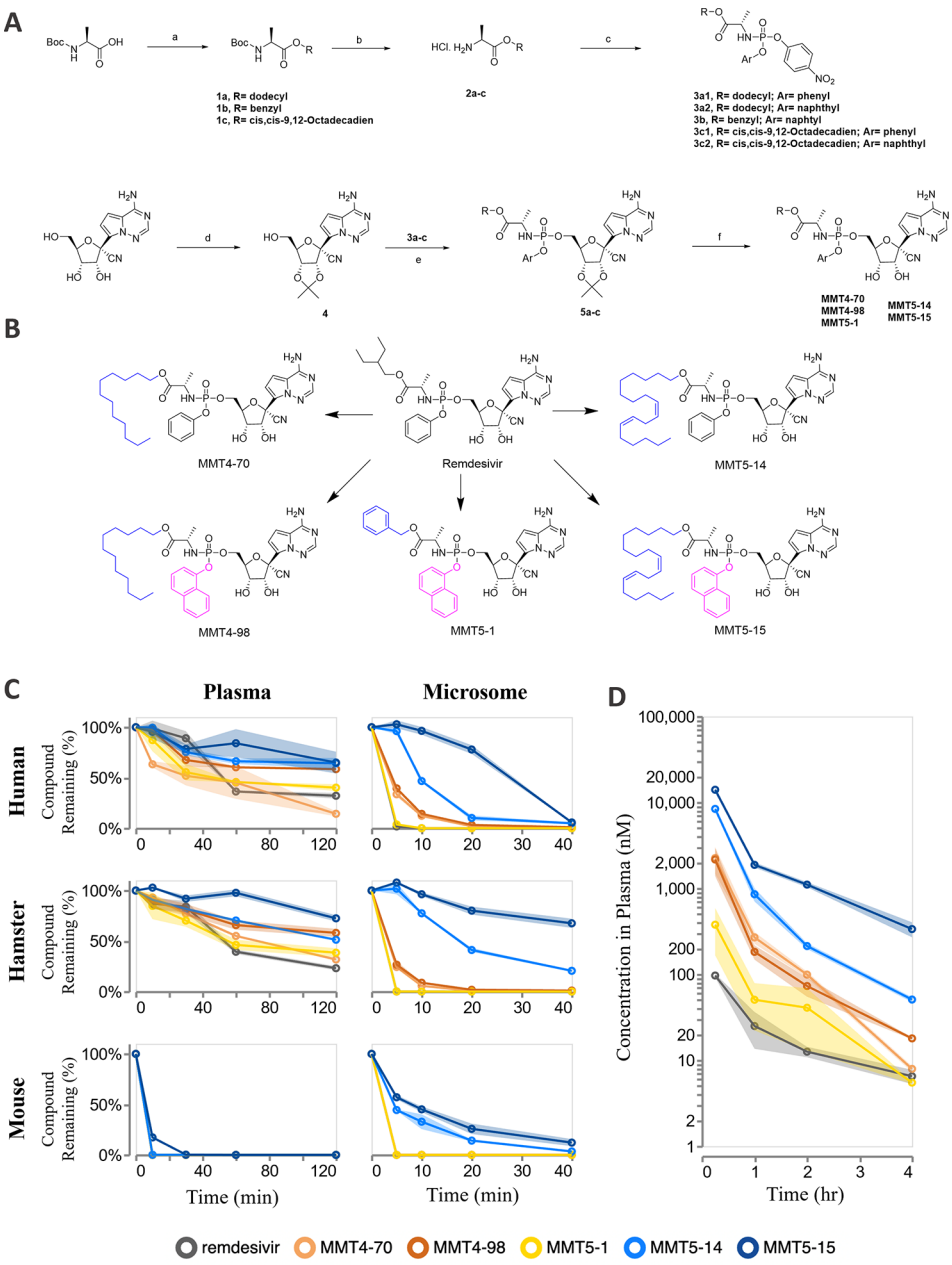

Figure 1. Synthesis of remdesivir analogues and their improved in vitro and in vivo stability. (A) Modification of prodrug moiety of remdesivir using the ProTide strategy. Reaction conditions: (a) appropriate alcohol, EDC, HCl, DMAP, CH_2Cl_2, rt, overnight, and 95%; (b) 4 M HCl in dioxane, rt, 4 h; (c) $OP(OAr)Cl_2$, ET_3N, CH_2Cl_2, −78 °C, 2 h, then 4-nitrophenol, ET_3N, 0 °C, 2 h, and 60%; (d) 2,2-dimethoxypropane, H_2SO_4, acetone, rt, 1.5 h, and 96%; (e) $MgCl_2$, DIPEA, MeCN, 2 h, 50 °C, and 74%; and (f) 37% HCl, THF, rt, 5 h, and 60%. (B) Structure of five new analogues in comparison with remdesivir. (C) In vitro plasma and microsome stability for remdesivir and its analogues in human, hamster, and mouse species. Data are represented as mean ± SD (shaded area). (D) In vivo plasma concentration−time profile in hamster of five new analogues in comparison with remdesivir (10 mg/kg, iv). Concentration of new analogues was normalized by scaling to the same molar dosage with remdesivir.

remdesivir to nucleoside metabolite (NUC, GS-441524) in the plasma may limit its antiviral activity since NUC is 20-fold less potent than remdesivir.[13] Due to the abundance of esterases and phosphatases in the plasma, NUC is the predominant metabolite (100-fold higher than remdesivir) in the plasma after injection of remdesivir.[12,14] (2) Low exposure of remdesivir and its active metabolite NTP in the SARS-CoV-2-targeted tissues (such as lungs) may limit its clinical efficacy. For instance, remdesivir was undetectable in the lungs, and only a low concentration of NTP was detected in the lungs after IV injection.[15,16] (3) Remdesivir has a relatively low potency (IC_{50}) against SARS-CoV-2.[17,18] Although remdesivir showed IC_{50} against SARS-CoV-2 in Calu-3 cells at the nanomolar range, its IC_{50} in other cells is in the micromolar range.[19] Recently, several studies on optimizing remdesivir prodrug to improve its antiviral potency and/or biostability were reported. However, to the best of our knowledge, no study to improve all the listed shortcomings has been reported yet.

In this study, we aim to modify the ProTide design by optimizing the prodrug moiety of remdesivir with better stability, higher lung accumulation, and better antiviral

https://doi.org/10.1021/acs.jmedchem.2c00758
J. Med. Chem. XXXX, XXX, XXX−XXX

Table 1. In Vitro Stability Half-Life Time of New Analogues in Comparison with Remdesivir[a]

	$t_{1/2}$(min), mean ± SE					
	human		hamster		mouse	
	plasma	microsome	plasma	microsome	plasma	microsome
remdesivir	40.7 ± 1.11	0.86 ± 0.04	54.5 ± 3.39	0.48 ± 0.01	N.D.	N.D.
MMT5-1	52.4 ± 3.83	1.05 ± 0.03	55.8 ± 4.36	0.46 ± 0.01	N.D.	N.D.
MMT4-70	47.1 ± 5.29	4.29 ± 0.11	71.2 ± 2.09	2.72 ± 0.30	N.D.	N.D.
MMT4-98	153.7 ± 2.40	6.11 ± 0.15	158 ± 11.9	3.49 ± 0.09	N.D.	N.D.
MMT5-14	191.9 ± 39.9	8.33 ± 0.61	128 ± 2.16	16.2 ± 0.44	1.03 ± 0.02	8.65 ± 0.35
MMT5-15	285.9 ± 137	19.7 ± 0.44	271 ± 37.8	61.82 ± 8.12	3.44 ± 0.06	13.6 ± 1.63

[a]Data are represented as mean ± SE, n = 3. N.D. None detected due to zero concentration of compounds due to rapid degradation.

activities. For that purpose, the following strategy was adopted to optimize these compounds: (1) since the activation of remdesivir starts with the hydrolysis of the L-alanine ester followed by an intramolecular displacement of the phenolate moiety to generate the alanine metabolite (ALA), modifications on these two positions with bulky moieties would likely improve its stability;[11,20] (2) long lipid chain modification in molecular structure may improve drug exposure/selectivity in the lungs;[21] and (3) linoleic acid (LA) moiety has been shown to inhibit spike protein and angiotensin-converting enzyme 2 (ACE 2) receptor that may further improve the anti-SARS-CoV-2 activity.[22] It is known that premature activation of remdesivir to NUC reduces its antiviral activity[13] and that a more stable ProTide prodrug could potentially slow down its activation and also reduce its activity. The optimized compound MMT5-14, which is 3- to 8-fold more stable than remdesivir in the plasma and liver microsome, not only achieved 10- to 500-fold higher drug concentration and 4- to 5-fold higher active metabolite (NTP) in the target tissues (e.g., lungs) but also demonstrated 2- to 7-fold higher antiviral activity against four SARS-CoV-2 variants (alpha, beta, gamma, and delta) compared to remdesivir. Therefore, MMT5-14 may have the potential to treat COVID-19 with severe symptoms.

RESULTS AND DISCUSSION

Modification of Prodrug Moiety of Remdesivir to Generate New Analogues. Five new derivatives were synthesized by modifying the prodrug moiety of remdesivir in ProTide as described in Figure 1A. First, esterification of N-Boc-L-alanine with appropriate alcohols (1-dodecanol, benzyl alcohol, and *cis*,*cis*-9,12-octadecadien-1-ol) provided compounds **1a**−**c**, which were subsequently taken into 4 M HCl for Boc deprotection to afford intermediates **2** as a salt. Condensation of intermediates **2** with either phenyl or naphthyl dichlorophosphate, followed by 4-nitrophenol, afforded intermediates **3** at the phosphorus. Acetonide protection of the 2′,3′-hydroxyl moieties of nucleoside with 2,2-dimethoxypropane in the presence of H_2SO_4 afforded the intermediate **4**. Coupling of intermediate **4** with intermediates **3** in the presence of magnesium chloride and Hünig's base efficiently afforded the intermediates **5**. The last step consisted of the acetonide group deprotection of intermediates **5** and provided the final compounds in good yields (Figure 1B). The NMR spectra and HPLC chromatograms of these compounds are provided in Figure S1.

In Vitro Plasma and Microsomal Stability and In Vivo Stability of New Analogues in Comparison with Remdesivir. To select more stable analogues in plasma and liver microsomes, we tested the five newly synthesized analogues for their stability in plasma and liver microsomes in three different species: human, hamster, and mouse. As shown in Figure 1C and Table 1, in comparison with MMT5-14 and MMT4-70 with a similar scaffold, MMT5-14 with the linoleyl alcohol chain improved the plasma stability in human and hamster by 3- to 4-fold, while MMT4-70 with the C12 alkyl chain failed to do so. In comparison of MMT5-15, MMT4-98, and MMT5-1, both MMT5-15 and MMT4-98 improved the stability by 3- to 4-fold in human and hamster plasma, while MMT5-1 failed to do so. All compounds degraded rapidly in mouse plasma due to the abundant esterases in mouse plasma. This difference in stability was even more significant in liver microsomes. MMT5-14 and MMT5-15 showed the higher stability than remdesivir in the microsomes of all the three species ($t_{1/2}$ was 8−20 min in human, 16−60 min in hamster, and 10−13 min in mouse). MMT4-70 and MMT4-98 also degraded slower than remdesivir even though the stability difference was less significant. MMT5-1 showed no difference with remdesivir in microsomal stability.

To further test the stability of these compounds in vivo, all the five compounds and remdesivir were dosed in hamster (10 mg/kg) to measure the plasma concentration. As shown in Figure 1D, MMT5-14 and MMT5-15 achieved the highest concentration in plasma, followed by the 12-carbon-chain-modified analogues, MMT4-70 and MMT4-98. Remdesivir was metabolized rapidly with 10- to 100-fold less concentration when compared to MMT5-14 or MMT5-15.

MMT5-14 and MMT5-15 Achieved Higher Concentrations of Both Prodrugs and Active Metabolites (NTP) in Blood and Lungs. The ProTide type of prodrugs needs to not only achieve high drug concentration but also generate high concentration of the active metabolite (NTP) in the targeted tissues (e.g., lungs) after these prodrugs were dosed in vivo. To select the best lead compound to achieve these goals, we also measured the intact prodrug, alanine metabolite (ALA), released nucleoside (NUC), and active metabolite triphosphate of nucleoside (NTP) after in vivo IV dosing (10 mg/kg) (Figure 2A). As shown in Figure 2B, three compounds, MMT5-14, MMT5-15, and MMT4-98, showed 8- to 10-fold higher intact prodrug concentration than remdesivir in the lungs at 4 h post IV dosing. In addition, these three compounds also generated 2- to 4.5-fold higher NTP in the lungs than remdesivir. MMT5-14 showed the highest level of NTP in the lungs in comparison with other compounds and thus was selected for further studies (Figure 2B).

We generated two different formulations (cyclodextrin formulation and albumin nanoparticle) of MMT5-14 in

https://doi.org/10.1021/acs.jmedchem.2c00758
J. Med. Chem. XXXX, XXX, XXX−XXX

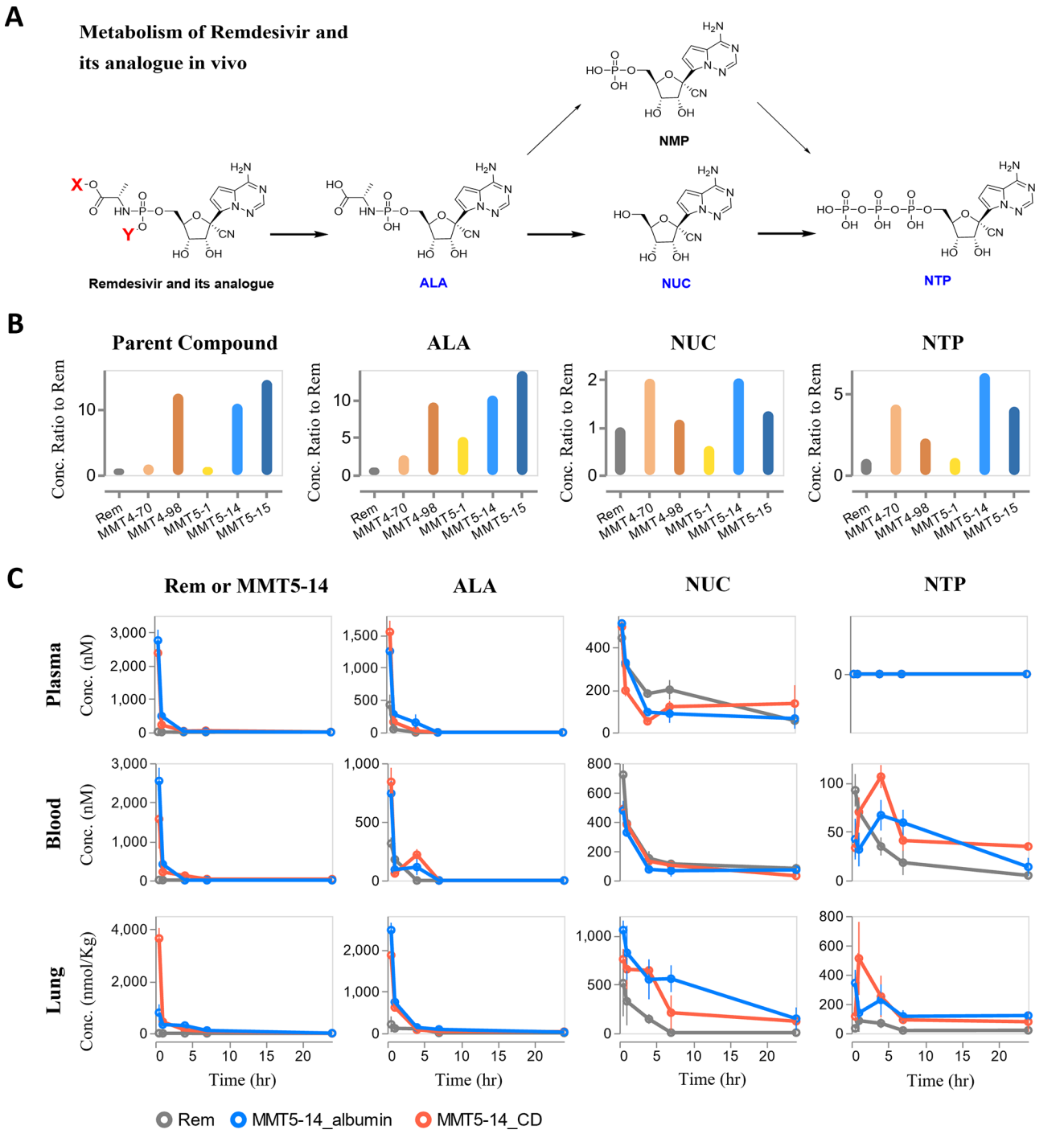

Figure 2. (A) Activation of prodrug remdesivir and formation of its active metabolite NTP in vivo. (B) Ratio of compound concentration in lungs between new analogues and remdesivir (10 mg/kg, iv, 4 h). (C) Concentration−time profile of MMT5-14 (two formulations) and its metabolites in the plasma, blood, and lungs in comparison with remdesivir after 10 mg/kg IV dose in hamsters.

comparison with clinical formulation of remdesivir in a detailed PK study. As shown in Figure 2C, both formulations of MMT5-14 increased the plasma concentration of MMT5-14 (more than 300-fold) and decreased the NUC formation by 2-fold in the plasma. Since NTP is only formed inside the cells, no NTP was observed in the plasma. Interestingly, MMT5-14 increased intact prodrug concentration, ALA, and NUC in the blood and lungs by 2- to10-fold (in blood) and by 4- to 200-fold (in the lungs). These data suggest that more MMT5-14 is accumulated than remdesivir into these tissues. More importantly, MMT5-14 generated 4.5-fold higher active metabolite NTP in the lungs and 2-fold higher NTP in the blood compared to remdesivir.

MMT5-14 Not Only Increased Tissue Exposure but Also Increased the Tissue Selectivity of Both Prodrug and Active Metabolite NTP in the Lungs, Spleen, and Blood. The drug's activity is usually correlated with drug exposures in the disease-targeted tissues.[23,24] To compare the drug exposure in various tissues of MMT5-14 and remdesivir, we calculated and compared the AUC of prodrug, ALA, NUC, and NTP in all tissues (Figures S2, S3). Their exposure (AUC) ratios between MMT5-14 and remdesivir group are shown in

https://doi.org/10.1021/acs.jmedchem.2c00758
J. Med. Chem. XXXX, XXX, XXX−XXX

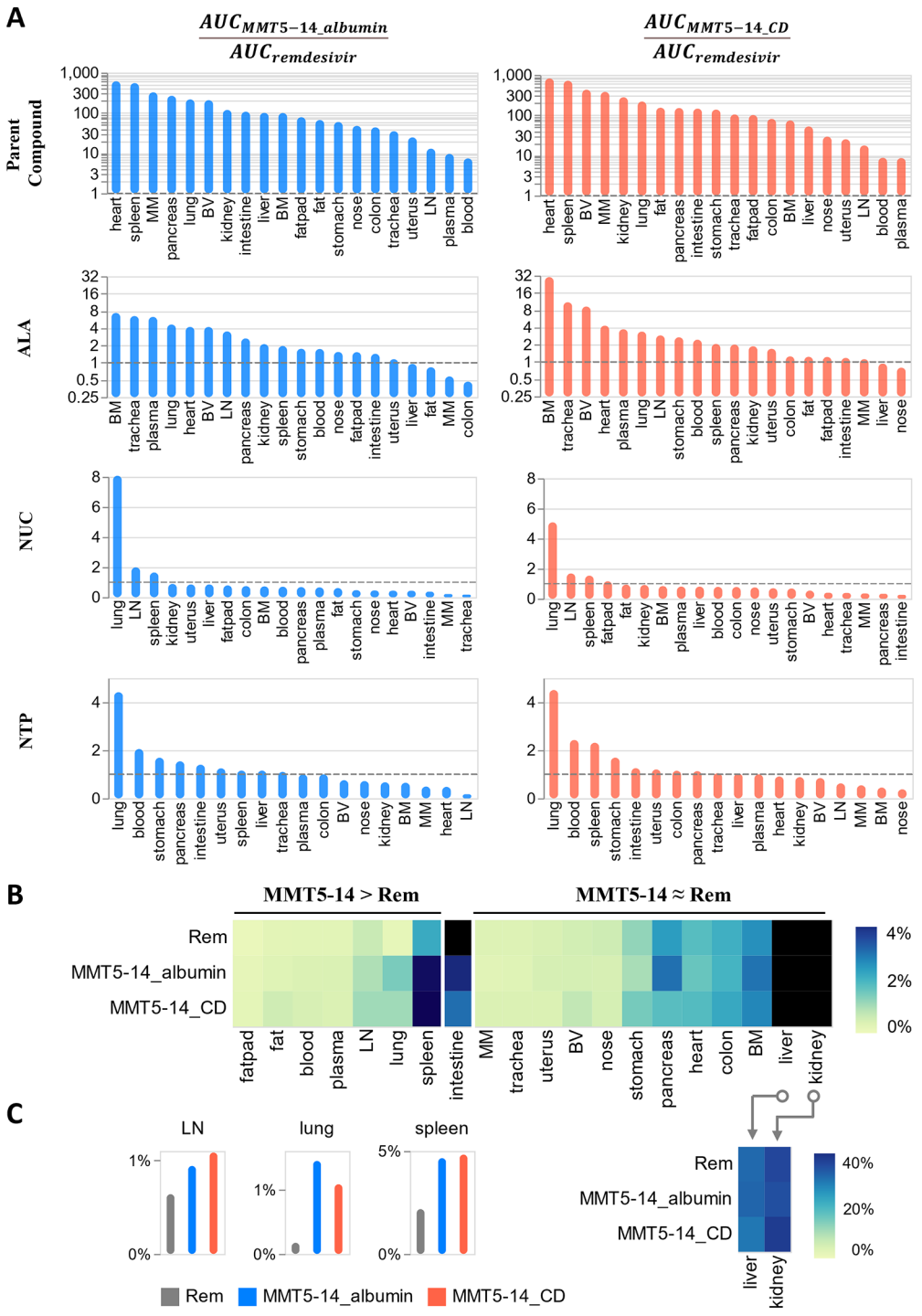

Figure 3. (A) Drug exposure (AUC) ratios of prodrug, ALA, NUC, and NTP between MMT5-14 and remdesivir after IV dose (10 mg/kg, iv, in hamsters). (B) Comparison of tissue selectivity in all tissues between MMT5-14 and remdesivir. (C) MMT5-14 increased the tissue selectivity in the lungs, spleen, and lymph nodes.

Figure 3A. The exposure (AUC) ratios of MMT5-14 (both albumin and cyclodextrin formulations) versus remdesivir were in the range from 8 to 800 in various tissues, which suggest that MMT5-14 was able to increase tissue exposure in most of the tissues. In comparison, the AUC ratio of metabolite ALA from MMT5-14 versus remdesivir was also 1- to 8-fold higher in most tissues.

However, the exposure (AUC) ratios of NUC and NTP from MMT5-14 versus remdesivir were very different. Higher exposure ratios of NUC from MMT5-14 versus remdesivir were only observed in the lungs, spleen, and lymph nodes (Figure 3A). More importantly, the higher exposure ratios of the active metabolite NTP from MMT5-14 versus remdesivir were only seen in the lungs, spleen, and blood (2 to 4.5-fold), which may provide advantage for its activity in these organs.

Further, the balance of drug efficacy/toxicity is often related to the drug tissue selectivity as calculated by the following equation.[23,24]

https://doi.org/10.1021/acs.jmedchem.2c00758
J. Med. Chem. XXXX, XXX, XXX−XXX

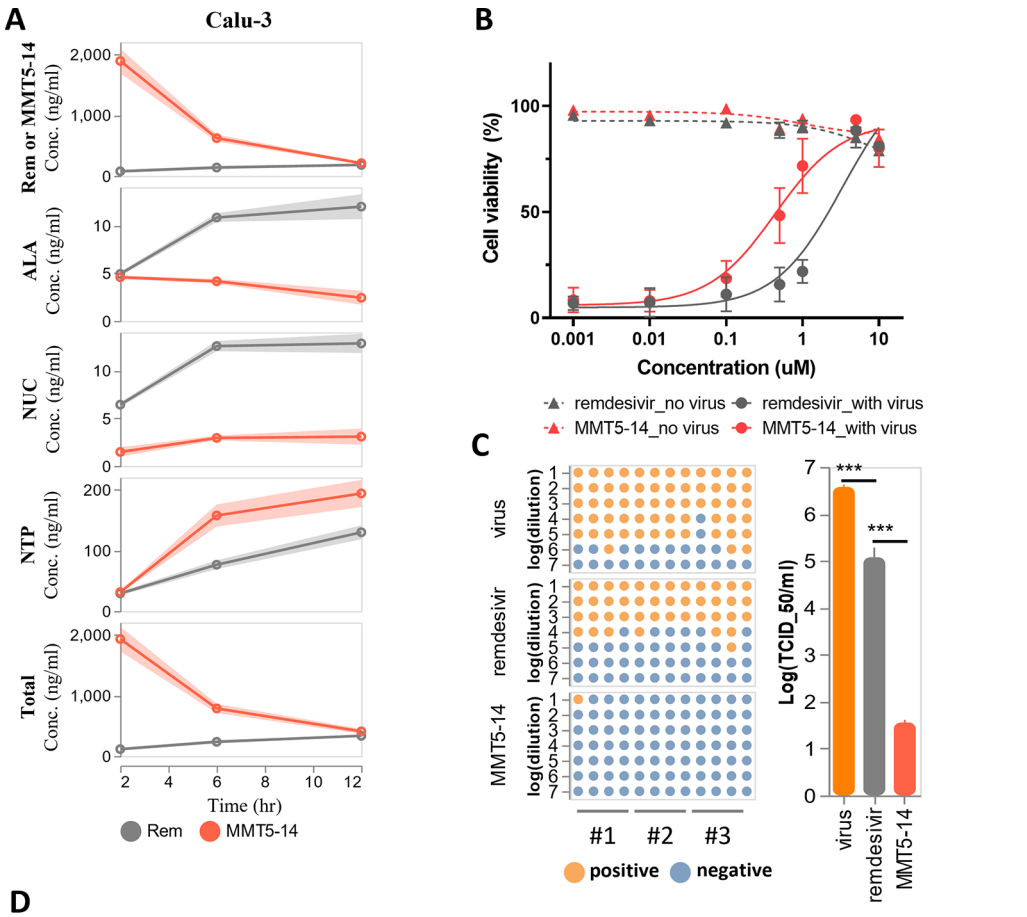

D

	EC_{50} (μM)				
	SARS-CoV-2	Alpha (B.1.1.7)	Beta (B.1.351)	Gamma (P.1)	Delta (B.1.617.2)
remdesivir	3.3	4.7	32.0	3.7	9.2
MMT5-14	0.4	2.5	15.9	1.7	5.6

Figure 4. (A) Intracellular uptake and activation of MMT5-14 and remdesivir (10 μM) in Calu-3. Data are represented by mean ± SD (shaded area). (B) Cell viability protection by MMT5-14 and remdesivir from SARS-CoV-2 virus infection. (C) Virus titer reduction assay by 5 μM of MMT5-14 or remdesivir. Data are represented by mean ± SD, ***$p < 0.001$, by two-tailed, unpaired t-test. (D) Calculated EC_{50} against SARS-CoV-2 virus and its variants for remdesivir and MMT5-14.

$$\text{Tissue selectivity}_{\text{i, compound}} = \frac{\text{AUC}_{\text{i, compound}}}{\sum_{\text{all}} \text{AUC}_{\text{all, compound}}}$$

where AUC_i represents the AUC of the compound in specific tissue i and $\sum AUC_{all}$ represents the sum of AUC of the compound in all tissues. Since the metabolism pathway (from prodrug to NTP) could influence the actual distribution of MMT5-14 or remdesivir, we added the AUC of all compounds together to calculate the tissue selectivity (Figure 3B,C). Surprisingly, MMT5-14 showed 5- to 10-fold higher tissue selectivity in lungs compared to remdesivir. Increased tissue selectivity could also be observed in the spleen (2-fold) and lymph nodes (1- to 2-fold).

It is worth noting that although both MMT5-14 and remdesivir had large percentage of accumulation in the kidney and liver (around 80% in total) and MMT5-14 increased prodrug exposure in these two organs in comparison with remdesivir, MMT5-14 neither increased NTP nor NUC in comparison with remdesivir (Figure 3A). Since it is possible that remdesivir's toxicity is related to high level of NUC and NTP in the kidney and liver (Figure S3), the preferred tissue exposure and selectivity of MMT5-14 and NTP may provide advantage to balance the efficacy and toxicity in the future clinical patients. We also dosed MMT5-14 (two formulations, 15 mg/kg) by intravenous administration for continuous 9 days. No obvious toxicity was observed in the hamsters.

MMT5-14 Increased Epithelial Cell Uptake. The cell uptake and intracellular activation of MMT5-14 and remdesivir were also performed in lung epithelial cell line Calu-3 in vitro (Figure 4A and Table S1). As expected, a much higher (100-fold) intracellular concentration of MMT5-14 was observed than remdesivir. However, the intracellular concentrations of ALA and NUC from MMT5-14 were 2- to 4-fold lower than that from remdesivir. In contrast, the intracellular level of NTP from MMT5-14 was 1- to 2-fold higher than that from remdesivir. The total intracellular concentration of MMT5-14 and its metabolites was 16-fold higher than that of remdesivir.

https://doi.org/10.1021/acs.jmedchem.2c00758
J. Med. Chem. XXXX, XXX, XXX−XXX

MMT5-14 Demonstrated Better In Vitro Antiviral Activity than Remdesivir. The antiviral activities of both MMT5-14 and remdesivir were evaluated against four variants of SARS-CoV-2 in Vero-E6 cells (Figure 4B). MMT5-15 showed 7-fold higher antiviral activity (7-fold lower EC_{50}) compared to remdesivir against SARS-CoV-2 as measured by the protection of Vero-E6 cell survival after infection of the virus. MMT5-14 is also active against other four variants (alpha, beta, gamma, and delta), which showed 2- to 7-fold higher activity than remdesivir. Both MMT5-14 and remdesivir alone showed very little toxicity in Vero-E6 cells at concentration up to 10 μM.

The virus titer reduction by MMT5-14 versus remdesivir was further evaluated as shown in Figure 4C. A series of dilutions of culture medium with virus alone, remdesivir and virus, or MMT5-14 and virus were incubated with Vero-E6 cells. The virus-infected cells with low cell viability in the presence/absence of drug treatment were labeled positive. The quantification of the titer reduction was also calculated by $\log(TCID_{50}/mL)$ //through the Reed−Muench method[25]

$$\Delta\text{logs} = (\text{endpoint dilution}) + \Delta\text{logs}\cdot(\text{dilution factor})$$

$$\Delta\text{logs} = [(\text{infection ratio at endpoint dilution}) - 50\%] / [(\text{infection ratio at endpoint dilution}) - (\text{infection ratio after endpoint dilution})]$$

The endpoint dilution represents the dilution times with infection ratio above 50%. MMT5-14 showed 4-fold higher virus titer reduction than remdesivir as measured by the significant decrease of log10 (TCID50).

CONCLUSIONS

Despite the recent successful development of antiviral therapy for mild and moderate COVID-19 patients, COVID-19 patients with severe symptoms still lack effective antiviral treatment. Although remdesivir is the only FDA-approved drug in treating severe symptoms of COVID-19, its efficacy is limited by premature hydrolysis to NUC, low accumulation in the disease-targeted tissues (e.g., lungs), and low antiviral potency. In this study, we synthesized new series prodrugs of RdRp inhibitor by modifying the prodrug moiety of remdesivir using the ProTide strategy. The lead compound MMT5-14, in comparison with remdesivir, showed 2- to 7-fold antiviral activity than remdesivir in four variants of SARS-CoV-2 (alpha, beta, gamma, and delta). MMT5-14 increased the prodrug concentration by 300-fold and 200-fold in the plasma and lungs by reducing premature hydrolysis to NUC in hamsters, enhanced accumulation of active metabolite NTP in the lungs by 5-fold in hamster. MMT5-14 increased the intracellular uptake and activation in lung epithelial cells by 200-fold compared to remdesivir. These data suggest that MMT5-14 is a potential antiviral drug to treat COVID-19 patients with severe symptoms.

EXPERIMENTAL SECTION

Chemistry. All commercially available products and solvents were purchased from Sigma-Aldrich, AK Scientific, DC Chemicals, and Fisher Scientific. Solvents were used as received or dried over molecular sieves (4 Å). All water- or air-sensitive reactions were performed under an argon atmosphere with dry solvents and anhydrous conditions. All reactions were monitored by thin-layer chromatography (TLC) performed on aluminum-backed silica plates (0.2 mm, 60 F254). Purification by flash chromatography was performed on Merck silica gel 60 (230−400 mesh). Yields refer to chromatographically and spectroscopically (^{1}H and ^{31}P NMR) homogeneous materials, unless otherwise stated.

NMR spectra were recorded on a Bruker instrument (500 or 300 MHz) and calibrated using a solvent peak as an internal reference. The spectra were processed using MestReNova software. Chemical shifts δ are given in ppm and coupling constants (J) in Hz. Peak multiplicities are described as follows: s, singlet, t, triplet, and m, multiplet. High-resolution mass spectra were obtained on an AB Sciex X500R QTOF spectrometer. The purity of all compounds subjected to biological tests was determined by analytical HPLC and was found to be ≥95%.

The synthesis and characterization of compounds **4**[26] and **1b**[27] have been previously described.

General Method 1. The alcohol was dissolved in CH_2Cl_2 and cooled to 0 °C. A catalytic amount of DMAP (10%) was added, and the reaction mixture was stirred for 20 min at 0 °C. N-Boc-L-alanine (1eq) and EDC·HCl (1 equiv) were added to the reaction mixture at 0 °C. The mixture was stirred for 1 h, warmed up to room temperature, stirred overnight, and monitored by TLC. Upon completion, the mixture was diluted with CH_2Cl_2, washed with aqueous $NaHCO_3$, followed by brine and dried over Na_2SO_4. The solvent was concentrated under vacuum, and the residue was purified by silica gel column chromatography to provide compound **1**.

*Dodecyl (tert-Butoxycarbonyl)-L-alaninate (**1a**).* Compound **1a** (1.48 g, yield 86%) was obtained following General Method 1. ^{1}H NMR (500 MHz, methanol-d_4): δ 4.04−3.92 (m, 3H), 1.58−1.46 (m, 2H), 1.34 (s, 9H), 1.31−1.18 (m, 21H), 0.80 (t, J = 6.9 Hz, 3H). HRMS (ESI) m/z: 380.2726 [M + Na$^+$].

*(9Z,12Z)-Octadeca-9,12-dien-1-yl (Tert-butoxycarbonyl)-L-alaninate (**1c**).* Compound **1c** (5.12 g, yield 95%) was obtained following General Method 1. ^{1}H NMR (300 MHz, DMSO): δ 5.32 (q, J = 5.9 Hz, 4H), 4.17−3.81 (m, 4H), 2.73 (t, J = 5.9 Hz, 2H), 2.14−1.89 (m, 4H), 1.64−1.13 (m, 30H), 0.96−0.72 (m, 3H). HRMS (ESI) m/z: 460.3356 [M + Na$^+$].

General Method 2. Compound **1** was added in one portion to a solution of HCl/dioxane (4 mL, 4 M) cooled to 0 °C under argon. The ice bath was removed, and the mixture was continually stirred at room temperature for 4 h. Upon completion, the reaction mixture was condensed by rotary evaporation under high vacuum. The residue was then taken into dry Et_2O and collected by filtration to afford the deprotected alanine ester as a hydrochloride salt.

The alanine ester hydrochloride (1.1 equiv) and the aryloxy dichlorophosphate (1 equiv) were dissolved in anhydrous CH_2Cl_2 and cooled to −78 °C under argon. Et_3N (5 equiv) was added dropwise, and the reaction was allowed to slowly warm to room temperature and stirred for 2 h. The mixture was then cooled to 0 °C, and 4-nitrophenol (1 equiv) was added followed by the slow addition of Et_3N (1.1 equiv). The resulting mixture was allowed to slowly warm to room temperature and stirred for 3 h. Upon completion, the solvent was evaporated under reduced pressure, and the resulting residue was dissolved in anhydrous Et_2O and filtered. The solvent was concentrated under vacuum, and the residue was purified by silica gel column chromatography to provide compound **3** as a diastereoisomeric mixture.

*Dodecyl ((4-Nitrophenoxy)(phenoxy)phosphoryl)-L-alaninate (**3a1**).* Compound **3a1** (995.4 mg, yield 60%) was obtained as an ∼1:1 diastereomeric mixture following General Method 2. ^{1}H NMR (500 MHz, methanol-d_4): δ 8.18 (dd, J = 9.1, 1.8 Hz, 2H), 7.40−7.31 (m, 2H), 7.31−7.25 (m 2H), 7.22−7.09 (m, 3H), 4.06−3.85 (m, 3H), 1.54−1.35 (m, 2H), 1.32−1.08 (m, 21H), 0.79 (t, J = 6.9 Hz, 3H). ^{31}P NMR (202 MHz, methanol-d_4): δ −1.52, −1.80. HRMS (ESI) m/z: 535.2487 [M + H$^+$].

*Dodecyl ((Naphthalen-1-yloxy)(4-nitrophenoxy)phosphoryl)-L-alaninate (**3a2**).* Compound **3a2** (554 mg, yield 56%) was obtained as an ∼1:1 diastereomeric mixture following General Method 2. ^{1}H NMR (500 MHz, methanol-d_4): δ 8.19−8.12 (m, 2H), 8.06−7.96 (m, 1H), 7.82−7.76 (m, 1H), 7.63 (dd, J = 8.4, 2.9 Hz, 1H), 7.48−7.31 (m, 6H), 4.08−3.96 (m, 1H), 3.96−3.83 (m, 2H), 1.47−1.30 (m,

https://doi.org/10.1021/acs.jmedchem.2c00758
J. Med. Chem. XXXX, XXX, XXX−XXX

2H), 1.28−0.96 (m, 22H), 0.79 (td, J = 7.1, 1.5 Hz, 3H). ^{31}P NMR (202 MHz, methanol-d_4): δ −1.40, −1.43. HRMS (ESI) m/z: 585.2642 [M + H$^+$].

*Benzyl ((Naphthalen-1-yloxy)(4-nitrophenoxy)phosphoryl)-L-alaninate (**3b**).* Compound **3b** (438 mg, yield 34%) was obtained as an ∼1:1 diastereomeric mixture following General Method 2. ^{1}H NMR (500 MHz, methanol-d_4): δ 8.07 (dq, J = 8.9, 3.4 Hz, 2H), 8.02−7.95 (m, 1H), 7.84−7.72 (m, 1H), 7.62 (d, J = 8.2 Hz, 1H), 7.45−7.35 (m, 3H), 7.35−7.22 (m, 3H), 7.21−7.11 (m, 5H), 5.03−4.86 (m, 2H), 4.16−4.00 (m, 1H), 1.23 (dt, J = 7.2, 1.4 Hz, 3H). ^{31}P NMR (202 MHz, methanol-d_4): δ −1.33, −1.50. HRMS (ESI) m/z: 507.1236 [M + H$^+$].

*(9Z,12Z)-Octadeca-9,12-dien-1-yl ((4-Nitrophenoxy) (phenoxy)-phosphoryl)-L-alaninate (**3c1**).* Compound **3c1** (916 mg, yield 61%) was obtained as an ∼1:1 diastereomeric mixture following General Method 2. ^{1}H NMR (500 MHz, methanol-d_4): δ 8.17−8.11 (m, 2H), 7.39−7.30 (m, 2H), 7.30−7.22 (m, 2H), 7.20−7.06 (m, 3H), 5.28−5.15 (m, 4H), 4.71 (s, 1H), 4.00−3.89 (m, 3H), 2.65 (t, J = 6.2 Hz, 2H), 1.97−1.86 (m, 4H), 1.49−1.39 (m, 2H), 1.29−1.08 (m, 19H), 0.77 (t, J = 6.9 Hz, 3H). ^{31}P NMR (202 MHz, methanol-d_4): δ −1.62, −1.87. HRMS (ESI) m/z: 615.3113 [M + H$^+$].

*(9Z,12Z)-Octadeca-9,12-dien-1-yl ((Naphthalen-1-yloxy)(4-nitrophenoxy)phosphoryl)-L-alaninate (**3c2**).* Compound **3c2** (673 mg, yield 42%) was obtained as an ∼1:1 diastereomeric mixture following General Method 2. ^{1}H NMR (500 MHz, methanol-d_4): δ 8.12 (d, J = 9.2 Hz, 2H), 8.05−7.96 (m, 1H), 7.80−7.71 (m, 1H), 7.64−7.56 (m, 1H), 7.49−7.27 (m, 6H), 5.28−5.14 (m, 4H), 4.10−3.96 (m, 1H), 3.94−3.81 (m, 2H), 2.64 (t, J = 6.3 Hz, 2H), 1.96−1.86 (m, 4H), 1.45−1.30 (m, 2H), 1.28−0.98 (m, 19H), 0.77 (t, J = 6.9 Hz, 3H). ^{31}P NMR (202 MHz, methanol-d_4): δ −1.44, −1.49. HRMS (ESI) m/z: 665.3284 [M + H$^+$].

General Method 3. To a solution of compound **3** (1.2 equiv) in CH_3CN was added compound **4** (1 equiv) and $MgCl_2$ (1 equiv) at room temperature. The solution was heated to 50 °C for 15 min, and DIPEA (2.5 equiv) was added. After 1 h, the reaction mixture was allowed to cool to room temperature and then diluted with EtOAc. The organic layer was washed with 5% aqueous citric acid, saturated aqueous NH_4Cl, 5% aqueous K_2CO_3, and brine. The organic layer was dried over anhydrous Na_2SO_4 and reduced to dryness to afford compound **5**, which was purified by column chromatography on silica gel.

*Dodecyl ((((3aR,4R,6R,6aR)-6-(4-aminopyrrolo[2,1-f][1,2,4]-triazin-7-yl)-6-cyano-2,2-dimethyltetrahydrofuro[3,4-d][1,3]dioxol-4-yl)methoxy)(phenoxy)phosphoryl)-L-alaninate (**5a1**).* Compound **5a1** (748.6 mg, yield 74%) was obtained as an ∼1:1 diastereomeric mixture following General Method 3. ^{1}H NMR (500 MHz, methanol-d_4): δ 7.76 (s, 1H), 7.20−7.12 (m, 2H), 7.07−7.01 (m, 2H), 6.97 (dt, J = 8.5, 1.3 Hz, 1H), 6.86−6.72 (m, 2H), 5.24 (d, J = 6.7 Hz, 1H), 4.90−4.81 (m, 1H), 4.54−4.43 (m, 1H), 4.27−4.12 (m, 2H), 4.00−3.85 (m, 2H), 3.77−3.64 (m, 1H), 1.60 (d, J = 3.9 Hz, 3H), 1.52−1.41 (m, 2H), 1.29 (d, J = 13.1 Hz, 3H), 1.17 (m, 23H), 0.79 (t, J = 6.9 Hz, 3H). ^{31}P NMR (202 MHz, methanol-d_4): δ 3.51, 3.20. HRMS (ESI) m/z: 727.3462 [M + H$^+$].

*Dodecyl ((((3aR,4R,6R,6aR)-6-(4-Aminopyrrolo[2,1-f][1,2,4]-triazin-7-yl)-6-cyano-2,2-dimethyltetrahydrofuro[3,4-d][1,3]dioxol-4-yl)methoxy)(naphthalen-1-yloxy)phosphoryl)-L-alaninate (**5a2**).* Compound **5a2** (347 mg, yield 70%) was obtained as an ∼1:1 diastereomeric mixture following General Method 3. ^{1}H NMR (500 MHz, methanol-d_4): δ 8.03−7.85 (m, 1H), 7.79−7.68 (m, 2H), 7.54 (dd, J = 32.4, 8.2 Hz, 1H), 7.41−7.13 (m, 4H), 6.81−6.67 (m, 2H), 4.92 (d, J = 6.6 Hz, 1H), 4.80 (dd, J = 6.6, 3.3 Hz, 1H), 4.47 (dt, J = 5.7, 3.9 Hz, 1H), 4.30−4.13 (m, 2H), 4.00−3.75 (m, 3H), 1.57 (d, J = 12.3 Hz, 3H), 1.50−1.35 (m, 2H), 1.27−0.99 (m, 26H), 0.78 (t, J = 7.1 Hz, 3H). ^{31}P NMR (202 MHz, methanol-d_4): δ 3.87, 3.64. HRMS (ESI) m/z: 777.3634 [M + H$^+$].

*Benzyl ((((3aR,4R,6R,6aR)-6-(4-Aminopyrrolo[2,1-f][1,2,4]triazin-7-yl)-6-cyano-2,2-dimethyltetrahydrofuro[3,4-d][1,3]dioxol-4-yl)-methoxy)(naphthalen-1-yloxy)phosphoryl)-L-alaninate (**5b**).* Compound **5b** (260 mg, yield 67%) was obtained as an ∼1:1 diastereomeric mixture following General Method 3. ^{1}H NMR (500 MHz, methanol-d_4) δ 8.10−7.90 (m, 1H), 7.90−7.73 (m, 2H), 7.71−7.54 (m, 1H), 7.50−7.31 (m, 3H), 7.31−7.20 (m, 6H), 6.91−6.72 (m, 2H), 5.13−4.97 (m, 3H), 4.88−4.85 (m, 1H), 4.54−4.48 (m, 1H), 4.35−4.19 (m, 2H), 4.04−3.94 (m, 1H), 1.66 (d, J = 11.5 Hz, 3H), 1.34−1.20 (m, 6H); ^{31}P NMR (202 MHz, methanol-d_4): δ 3.91, 3.53. HRMS (ESI) m/z: 699.2217 [M + H$^+$].

*(9Z,12Z)-Octadeca-9,12-dien-1-yl ((((3aR,4R,6R,6aR)-6-(4-Aminopyrrolo[2,1-f][1,2,4]triazin-7-yl)-6-cyano-2,2-dimethyltetrahydrofuro[3,4-d][1,3]dioxol-4-yl)methoxy)(phenoxy)-phosphoryl)-L-alaninate (**5c1**).* Compound **5c1** (404 mg, yield 52%) was obtained as an ∼1:1 diastereomeric mixture following General Method 3. ^{1}H NMR (500 MHz, methanol-d_4): δ 7.76 (s, 1H), 7.25−7.10 (m, 2H), 7.07−7.01 (m, 2H), 6.97 (dq, J = 7.7, 1.2 Hz, 1H), 6.84−6.72 (m, 2H), 5.31−5.14 (m, 4H), 4.92−4.81 (m, 1H), 4.56−4.38 (m, 1H), 4.28−4.10 (m, 3H), 4.03−3.82 (m, 2H), 3.79−3.61 (m, 1H), 2.67 (t, J = 6.5 Hz, 1H), 2.01−1.86 (m, 3H), 1.60 (d, J = 3.9 Hz, 4H), 1.43−1.37 (m, 3H), 1.35−1.09 (m, 26H), 0.80 (t, J = 6.9 Hz, 3H). ^{31}P NMR (202 MHz, methanol-d_4): δ 3.51, 3.20. HRMS (ESI) m/z: 807.4087 [M + H$^+$].

*(9Z,12Z)-Octadeca-9,12-dien-1-yl ((((3aR,4R,6R,6aR)-6-(4-Aminopyrrolo[2,1-f][1,2,4]triazin-7-yl)-6-cyano-2,2-dimethyltetrahydrofuro[3,4-d][1,3]dioxol-4-yl)methoxy)-(naphthalen-1-yloxy)phosphoryl)-L-alaninate (**5c2**).* Compound **5c2** (436 mg, yield 68%) was obtained as an ∼1:1 diastereomeric mixture following General Method 3. ^{1}H NMR (500 MHz, methanol-d_4): δ 8.03−7.84 (m, 1H), 7.77−7.69 (m, 2H), 7.60−7.48 (m, 1H), 7.42−7.21 (m, 3H), 7.17 (t, J = 7.9 Hz, 1H), 6.82−6.67 (m, 2H), 5.32−5.13 (m, 4H), 4.93 (d, J = 6.6 Hz, 1H), 4.84−4.77 (m, 1H), 4.47 (qd, J = 4.1, 1.7 Hz, 1H), 4.31−4.11 (m, 2H), 4.01−3.78 (m, 3H), 2.73−2.58 (m, 2H), 2.00−1.83 (m, 4H), 1.57 (d, J = 11.9 Hz, 3H), 1.48−1.34 (m, 2H), 1.32−1.00 (m, 23H), 0.78 (t, J = 7.0 Hz, 3H). ^{31}P NMR (202 MHz, methanol-d_4): δ 3.85, 3.63. HRMS (ESI) m/z: 857.4227 [M + H$^+$].

General Method 4. To a stirred solution of intermediate **5** (1 equiv) in THF was added 37% aqueous HCl slowly at 0 °C. The reaction mixture was allowed to warm to room temperature. After 6 h, the reaction mixture was diluted with water and adjusted to pH = 8 by the addition of saturated aqueous $NaHCO_3$. The resulting mixture was extracted with EtOAc, and the organic layer was then washed with brine, dried over anhydrous Na_2SO_4, and concentrated under reduced pressure. The crude product obtained after evaporation was purified by column chromatography on silica gel to give the remdesivir analogue.

*Dodecyl ((((2R,3S,4R,5R)-5-(4-Aminopyrrolo[2,1-f][1,2,4]triazin-7-yl)-5-cyano-3,4-dihydroxytetrahydrofuran-2-yl)methoxy)-(phenoxy)phosphoryl)-L-alaninate (**MMT4-70**).* Compound **MMT4-70** (337.3 mg, yield 60%) was obtained as a diastereomeric mixture (45, 55%) following General Method 4.^{1}H NMR (500 MHz, methanol-d_4): δ 7.85 (d, J = 7.5 Hz, 1H), 7.29 (dt, J = 9.2, 7.2 Hz, 2H), 7.22−7.07 (m, 3H), 6.97−6.73 (m, 2H), 4.79 (d, J = 5.4 Hz, 1H), 4.45−4.33 (m, 2H), 4.33−4.24 (m, 1H), 4.18 (dt, J = 17.3, 5.5 Hz, 1H), 4.10−3.96 (m, 3H), 1.64−1.48 (m, 2H), 1.26 (tdd, J = 13.7, 5.7, 2.2 Hz, 25H), 0.89 (t, J = 6.8 Hz, 3H); ^{31}P NMR (202 MHz, methanol-d_4): δ 3.53 (s), 3.49 (s); HRMS (ESI) m/z: 687.3160 [M + H$^+$].

*Dodecyl ((((2R,3S,4R,5R)-5-(4-Aminopyrrolo[2,1-f][1,2,4]triazin-7-yl)-5-cyano-3,4-dihydroxytetrahydrofuran-2-yl)methoxy)-(naphthalen-1-yloxy)phosphoryl)-L-alaninate (**MMT4-98**).* Compound **MMT4-98** (75 mg, yield 26%) was obtained as a diastereomeric mixture (47, 53%) following General Method 4. ^{1}H NMR (500 MHz, methanol-d_4): δ 8.16−8.02 (m, 1H), 7.87−7.79 (m, 2H), 7.66 (t, J = 8.0 Hz, 1H), 7.53−7.40 (m, 3H), 7.34 (dt, J = 9.5, 7.9 Hz, 1H), 6.88−6.76 (m, 2H), 4.69 (t, J = 5.6 Hz, 1H), 4.46 (dddd, J = 11.4, 8.9, 6.0, 2.8 Hz, 1H), 4.41−4.30 (m, 2H), 4.19 (t, J = 5.5 Hz, 1H), 4.04−3.90 (m, 3H), 1.58−1.43 (m, 2H), 1.37−1.09 (m, 25H), 0.89 (t, J = 6.8, 3H); ^{31}P NMR (202 MHz, methanol-d_4): δ 3.92 (s), 3.87 (s); HRMS (ESI) m/z: 737.3362 [M + H$^+$].

*Benzyl ((((2R,3S,4R,5R)-5-(4-Aminopyrrolo[2,1-f][1,2,4]triazin-7-yl)-5-cyano-3,4-dihydroxytetrahydrofuran-2-yl)methoxy)-(naphthalen-1-yloxy)phosphoryl)-L-alaninate (**MMT5-1**).* Compound **MMT5-1** (62.6 mg, yield 30%) was obtained as a diastereomeric mixture (42, 58%) following General Method 4. ^{1}H

https://doi.org/10.1021/acs.jmedchem.2c00758
J. Med. Chem. XXXX, XXX, XXX−XXX

NMR (500 MHz, methanol-d_4): δ 8.12−8.01 (m, 1H), 7.88−7.78 (m, 2H), 7.65 (dd, J = 10.7, 8.2 Hz, 1H), 7.52−7.36 (m, 3H), 7.35−7.20 (m, 6H), 6.91−6.71 (m, 2H), 5.09−4.95 (m, 2H), 4.67 (dd, J = 9.2, 5.5 Hz, 1H), 4.47−4.25 (m, 3H), 4.20−4.13 (m, 1H), 4.02−3.89 (m, 1H), 1.31−1.24 (m, 3H); ^{31}P NMR (202 MHz, methanol-d_4): δ 3.95 (s), 3.82 (s); HRMS (ESI) m/z: 659.1912 [M + H$^+$].

*(9Z,12Z)-Octadeca-9,12-dien-1-yl ((((2R,3S,4R,5R)-5-(4-Aminopyrrolo[2,1-f][1,2,4]triazin-7-yl)-5-cyano-3,4-dihydroxytetrahydrofuran-2-yl)methoxy)(phenoxy)phosphoryl)-L-alaninate (**MMT5-14**)*. Compound **MMT5-14** (169.6 mg, yield 51%) was obtained as a diastereomeric mixture (48, 52%) following General Method 4.^{1}H NMR (500 MHz, methanol-d_4): δ 7.85 (s, 1H), 7.29 (dt, J = 9.1, 7.4 Hz, 2H), 7.21−7.10 (m, 3H), 6.93−6.85 (m, 2H), 5.43−5.23 (m, 4H), 4.79 (d, J = 5.4 Hz, 1H), 4.47−4.33 (m, 2H), 4.33−4.23 (m, 1H), 4.19 (dt, J = 17.5, 5.5 Hz, 1H), 4.10−3.94 (m, 2H), 3.92−3.76 (m, 1H), 2.76 (t, J = 6.3 Hz, 2H), 2.11−1.98 (m, 4H), 1.60−1.52 (m, 2H), 1.41−1.19 (m, 23H), 0.89 (t, J = 6.8 Hz, 3H); ^{31}P NMR (202 MHz, methanol-d_4): δ 3.52 (s), 3.50 (s); HRMS (ESI) m/z: 767.3773 [M + H$^+$].

*(9Z,12Z)-Octadeca-9,12-dien-1-yl ((((2R,3S,4R,5R)-5-(4-Aminopyrrolo[2,1-f][1,2,4]triazin-7-yl)-5-cyano-3,4-dihydroxytetrahydrofuran-2-yl)methoxy)(naphthalen-1-yloxy)phosphoryl)-L-alaninate (**MMT5-15**)*. Compound **MMT5-15** (171.9 mg, yield 60%) was obtained as a diastereomeric mixture (50, 50%) following General Method 4. ^{1}H NMR (500 MHz, methanol-d_4): δ 8.09 (ddd, J = 24.8, 7.6, 2.2 Hz, 1H), 7.88−7.78 (m, 2H), 7.66 (t, J = 7.9 Hz, 1H), 7.52−7.46 (m, 2H), 7.46−7.40 (m, 1H), 7.38−7.28 (m, 1H), 6.87−6.77 (m, 2H), 5.43−5.18 (m, 4H), 4.69 (t, J = 5.5 Hz, 1H), 4.49−4.41 (m, 1H), 4.42−4.37 (m, 1H), 4.34 (td, J = 10.6, 10.0, 4.4 Hz, 1H), 4.19 (t, J = 5.5 Hz, 1H), 4.03−3.91 (m, 3H), 2.75 (t, J = 6.3 Hz, 2H), 2.09−1.91 (m, 4H), 1.55−1.42 (m, 2H), 1.39−1.07 (m, 23H), 0.89 (t, J = 6.8 Hz, 3H); ^{31}P NMR (202 MHz, methanol-d_4): δ 3.93 (s), 3.87(s); HRMS (ESI) m/z: 817.3939 [M + H$^+$].

Cells. Calu-3 (HTB-55) and Vero E6 cells were purchased from American Type Culture Collection. Calu-3 cells were cultured in ATCC-formulated Eagle's minimum essential medium (EMEM) supplemented with 10% fetal bovine serum. Humanumbilical veinendothelial cells (HUVECs) were cultured in vascular cell basal medium supplemented with Endothelial Cell Growth Kit-BBE (ATCC PCS-100-040, including bovine brain extract (BBE), rh EGF, L-glutamine, heparin sulfate, hydrocortisone hemisuccinate, fetal bovine serum, and ascorbic acid). Vero E6 cells were cultured in EMEM supplemented with 5% FBS.

Virus. Four variants (alpha, beta, gamma, and delta) of SARS-CoV-2 were isolated in UTHSC facility.

Animal. Catheterized LVG Golden Syrian Hamster (female, 70−80 g, Jugular vein catheters) are purchased from Charles river and used for PK study. All animal procedures used in this study were approved by the University Committee on Use and Care Animals at the University of Michigan.

PK Study. Catheterized female hamsters were used for PK study. Remdesivir (10 mg/Kg, 15% cyclodextrin, pH 3−3.5) and MMT5-14 (cyclodextrin or albumin formulation) were injected intravenously with the concentration set as 2 mg/mL. At scheduled time points (0.5, 1, 4, 7, and 24 h), two hamsters from each group were sacrificed and tissues including blood, blood vessels, bone marrow, brain, colon, fat, fat pad, heart, intestine, kidney, liver, lungs, lymph nodes, mouth membrane, muscle, nose, pancreas, plasma, skin, spleen, stomach, trachea, and uterus were collected and stored at −80 °C in a refrigerator. Before analyzing, the samples were mixed with 5-fold of 70% methanol solution (internal standard included) and homogenized within Precellys Lysing Kit (7700 rpm, 20 s * 4 per cycle, three cycles in total, 4 °C). The supernatant was then collected through centrifugation for further concentration test. Remdesivir, MMT5-14, ALA, and NUC were analyzed on an X500R QTOF System (AB Sciex, USA) (references). Chromatographic separation was obtained on a 50 × 2.1 mm Agilent 3.5 μm C18 column using a constant flow rate of 0.6 mL/min. The gradient mobile phase consisted of 0.1% formic acid in water (mobile phase A) and 0.1% formic acid acetonitrile (mobile phase B), running from 5% B to 95% B within 3 min and then maintaining 95% B for 1 min. The eluent was introduced into quadrupole time-of-flight mass spectrometry by electrospray ionization (ESI) operated in positive modes. For NTP analysis, the supernatant solution was further concentrated to 20-fold through freeze-drying, and its LC−MS/MS was performed by ion-pairing chromatography using LC 20AD UFLC (Shimadzu, Japan) coupling with an API 5500 (AB Sciex, USA). The separation was achieved on a 50 × 2.1 mm Agilent 3.5 μm C18 column. The mobile phase consisted of 3 mM ammonium formate with 10 mM dimethylhexylamine in water (mobile phase A) and 0.1% formic acid in ACN (mobile phase B). A multistage linear gradient initiated with 2% B for 1 min increased to 95% B in 2 min and maintained with 95% B for 1 min at a flow rate of 0.4 mL/min. Detection was performed in the negative ion mode and multiple reaction monitoring modes. All the analytes were quantified using 10-point standard curves ranging from 5 to 5000 ng/mL.

Cell Uptake. Calu-3 and HUVEC cells (1−5 * 10^5) were cultured per well in a 12-well plate for 12 h before incubating with drugs. Remdesivir or MMT5-14 (10 μM) was then added into each well and incubated at 37 °C for 2, 6, and 12 h (n = 3). At each scheduled time point, the medium was collected together with detached cells in trypsin−EDTA solution (200 μL per well). Centrifugation (600g, 5 min, 4 °C) was used to remove the medium, and the cell pellets were then washed with 1 mL ice-cold PBS three times. Ice-cold 70% methanol (200 μL) was added finally and stored at −20 °C overnight to extract the drug molecules. After centrifugation at 15,000g for 15 min, the supernatants were collected for LC−MS test.

In Vitro Antiviral Test against SARS-CoV-2. High-throughput screening (HTS) was used to provide the percent protection of the cytopathic effect of SARS-CoV-2.[28−32] Briefly, Vero E6 cells were plated into a 384-well plate with seeding density as 5000−6000 per well. The next day, different concentrations of compounds were added, and the highest DMSO was kept below 0.5%. The cells were transported to BSL-3 and inoculated with media or with SARS-CoV-2 with multiplicity of infection (MOI) as 0.1. After 2 days of incubation at 37 °C, 5% CO_2, 25 μL of Promega CellTiter-Glo (Promega, Madison, WI) was added to each well, and the luminescence was then measured using a PerkinElmer Envision plate reader (PerkinElmer, Wellesley, MA). Cells were only treated as the positive control and virus-infected cells as negative control as previously described. Titer reduction assay was used to show the different capacity of remdesivir and MMT5-14 in the reduction of the virus titer. Briefly, Vero E6 cells were grown in 12-well plates overnight and then infected 1 h with virus at a MOI of 0.1 diluted in EMEM. The cells were then washed twice with PBS and incubated with media containing 5 μM of remdesivir or MMT5-14. After 2 days, the supernatant was collected and the number of infectious virus particles in it was quantified by Median Tissue Culture Infectious Dose ($TCID_{50}$) assay. Vero E6 cells were used in this assay and incubated with serial dilution of the infectious supernatant (n = 4), and the cytopathic effect was monitored by Promega CellTiter-Glo kit.

■ ASSOCIATED CONTENT

Supporting Information

The Supporting Information is available free of charge at https://pubs.acs.org/doi/10.1021/acs.jmedchem.2c00758.

NMR spectra and HPLC trace of final compounds; PK profile of remdesivir and MMT5-14 in various tissues in hamster; AUC comparison between remdesivir and MMT5-14 for different tissues and metabolites; and intracellular uptake of MMT5-14 and formation of its metabolites in different cell lines (PDF)

Molecular formula strings (CSV)

https://doi.org/10.1021/acs.jmedchem.2c00758
J. Med. Chem. XXXX, XXX, XXX−XXX

AUTHOR INFORMATION

Corresponding Author

Duxin Sun − *Department of Pharmaceutical Sciences, College of Pharmacy, University of Michigan, Ann Arbor, Michigan 48109, United States;* orcid.org/0000-0002-6406-2126; Phone: 734-615-8740; Email: dxuins@umich.edu; Fax: 734-936-7675

Authors

Hongxiang Hu − *Department of Pharmaceutical Sciences, College of Pharmacy, University of Michigan, Ann Arbor, Michigan 48109, United States*

Mohamed Dit Mady Traore − *Department of Pharmaceutical Sciences, College of Pharmacy, University of Michigan, Ann Arbor, Michigan 48109, United States*

Ruiting Li − *Department of Pharmaceutical Sciences, College of Pharmacy, University of Michigan, Ann Arbor, Michigan 48109, United States*

Hebao Yuan − *Department of Pharmaceutical Sciences, College of Pharmacy, University of Michigan, Ann Arbor, Michigan 48109, United States;* orcid.org/0000-0003-4425-3678

Miao He − *Department of Pharmaceutical Sciences, College of Pharmacy, University of Michigan, Ann Arbor, Michigan 48109, United States*

Bo Wen − *Department of Pharmaceutical Sciences, College of Pharmacy, University of Michigan, Ann Arbor, Michigan 48109, United States*

Wei Gao − *Department of Pharmaceutical Sciences, College of Pharmacy, University of Michigan, Ann Arbor, Michigan 48109, United States;* orcid.org/0000-0002-5233-3734

Colleen B. Jonsson − *Department of Microbiology, Immunology and Biochemistry and the Regional Biocontainment Laboratory, University of Tennessee Health Science Center, Memphis, Tennessee 38163, United States;* orcid.org/0000-0002-2640-7672

Elizabeth A. Fitzpatrick − *Department of Microbiology, Immunology and Biochemistry and the Regional Biocontainment Laboratory, University of Tennessee Health Science Center, Memphis, Tennessee 38163, United States*

Complete contact information is available at: https://pubs.acs.org/10.1021/acs.jmedchem.2c00758

Author Contributions

M.M.T. and H.H. contributed to this work equally. M.M.T. designed and synthesized the compounds and wrote the manuscript. H.H. formulated the compounds and performed PK, data analysis, and wrote the manuscript. R.L. and B.W. analyzed the concentration of prodrugs and metabolites. H.Y. and H.M. helped with animal experiments. W.G. helped to analyze the data and revised the manuscript. C.B.J. and E.A.F. helped to measure the antiviral activity. D.S. conceived the idea and wrote the manuscript. All authors have given approval to the final version of the manuscript.

Notes

The authors declare no competing financial interest.

ACKNOWLEDGMENTS

This work was supported by the internal funding of the College of Pharmacy at University of Michigan.

ABBREVIATIONS

ACE 2, angiotensin-converting enzyme 2; ALA, alanine metabolite; CES 1, carboxylesterase 1; LA, linoleic acid; NMP, nucleoside monophosphate; NTP, nucleoside triphosphate; NUC, nucleoside metabolite; RdRp, RNA-dependent RNA polymerase

REFERENCES

(1) Jayk Bernal, A.; Gomes da Silva, M. M.; Musungaie, D. B.; Kovalchuk, E.; Gonzalez, A.; Delos Reyes, V.; Martín-Quirós, A.; Caraco, Y.; Williams-Diaz, A.; Brown, M. L.; Du, J.; Pedley, A.; Assaid, C.; Strizki, J.; Grobler, J. A.; Shamsuddin, H. H.; Tipping, R.; Wan, H.; Paschke, A.; Butterton, J. R.; Johnson, M. G.; De Anda, C.; MOVe-OUT Study Group. Molnupiravir for oral treatment of COVID-19 in nonhospitalized patients. *N. Engl. J. Med.* **2022**, *386*, 509−520.

(2) Mahase, E. COVID-19: Pfizer's paxlovid is 89% effective in patients at risk of serious illness, company reports. *Br. Med. J.* **2021**, *375*, n2713.

(3) Sanders, J. M.; Monogue, M. L.; Jodlowski, T. Z.; Cutrell, J. B. Pharmacologic treatments for coronavirus disease 2019 (COVID-19) a review. *JAMA, J. Am. Med. Assoc.* **2020**, *323*, 1824−1836.

(4) Eastman, R. T.; Roth, J. S.; Brimacombe, K. R.; Simeonov, A.; Shen, M.; Patnaik, S.; Hall, M. D. Remdesivir: a review of its discovery and development leading to emergency use authorization for treatment of COVID-19. *ACS Cent. Sci.* **2020**, *6*, 672−683.

(5) Beigel, J. H.; Tomashek, K. M.; Dodd, L. E.; Mehta, A. K.; Zingman, B. S.; Kalil, A. C.; Hohmann, E.; Chu, H. Y.; Luetkemeyer, A.; Kline, S.; Lopez de Castilla, D.; Finberg, R. W.; Dierberg, K.; Tapson, V.; Hsieh, L.; Patterson, T. F.; Paredes, R.; Sweeney, D. A.; Short, W. R.; Touloumi, G.; Lye, D. C.; Ohmagari, N.; Oh, M. D.; Ruiz-Palacios, G. M.; Benfield, T.; Fätkenheuer, G.; Kortepeter, M. G.; Atmar, R. L.; Creech, C. B.; Lundgren, J.; Babiker, A. G.; Pett, S.; Neaton, J. D.; Burgess, T. H.; Bonnett, T.; Green, M.; Makowski, M.; Osinusi, A.; Nayak, S.; Lane, H. C. Remdesivir for the treatment of COVID-19 - final report. *N. Engl. J. Med.* **2020**, *383*, 1813−1826.

(6) Wiersinga, W. J.; Rhodes, A.; Cheng, A. C.; Peacock, S. J.; Prescott, H. C. Pathophysiology, transmission, diagnosis, and treatment of coronavirus disease 2019 (COVID-19) a review. *JAMA, J. Am. Med. Assoc.* **2020**, *324*, 782−793.

(7) Pascarella, G.; Strumia, A.; Piliego, C.; Bruno, F.; Del Buono, R.; Costa, F.; Scarlata, S.; Agrò, F. E. COVID-19 diagnosis and management: a comprehensive review. *J. Intern. Med.* **2020**, *288*, 192−206.

(8) WHO Solidarity Trial Consortium. Repurposed antiviral drugs for COVID-19-interim WHO solidarity trial results. *N. Engl. J. Med.* **2021**, *384*, 497−511.

(9) Goldman, J. D.; Lye, D. C. B.; Hui, D. S.; Marks, K. M.; Bruno, R.; Montejano, R.; Spinner, C. D.; Galli, M.; Ahn, M. Y.; Nahass, R. G.; Chen, Y. S.; SenGupta, D.; Hyland, R. H.; Osinusi, A. O.; Cao, H. Y.; Blair, C.; Wei, X. L.; Gaggar, A.; Brainard, D. M.; Towner, W. J.; Muñoz, J.; Mullane, K. M.; Marty, F. M.; Tashima, K. T.; Diaz, G.; Subramanian, A.; Investigators, G.-U.-. Remdesivir for 5 or 10 days in patients with severe COVID-19. *N. Engl. J. Med.* **2020**, *383*, 1827−1837.

(10) Spinner, C. D.; Gottlieb, R. L.; Criner, G. J.; Arribas López, J. R. A.; Cattelan, A. M.; Soriano Viladomiu, A. S.; Ogbuagu, O.; Malhotra, P.; Mullane, K. M.; Castagna, A.; Chai, L. Y. A.; Roestenberg, M.; Tsang, O. T. Y.; Bernasconi, E.; Le Turnier, P.; Chang, S. C.; SenGupta, D.; Hyland, R. H.; Osinusi, A. O.; Cao, H. Y.; Blair, C.; Wang, H. Y.; Gaggar, A.; Brainard, D. M.; McPhail, M. J.; Bhagani, S.; Ahn, Y.; Sanyal, A. J.; Huhn, G.; Marty, F. M.; GS-US-540-5774 Investigators. Effect of remdesivir vs standard care on clinical status at 11 days in patients with moderate COVID-19 a randomized clinical trial. *JAMA, J. Am. Med. Assoc.* **2020**, *324*, 1048−1057.

(11) Kokic, G.; Hillen, H. S.; Tegunov, D.; Dienemann, C.; Seitz, F.; Schmitzova, J.; Farnung, L.; Siewert, A.; Höbartner, C.; Cramer, P.

Mechanism of SARS-CoV-2 polymerase stalling by remdesivir. *Nat. Commun.* **2021**, *12*, 279.
(12) Warren, T. K.; Jordan, R.; Lo, M. K.; Ray, A. S.; Mackman, R. L.; Soloveva, V.; Siegel, D.; Perron, M.; Bannister, R.; Hui, H. C.; Larson, N.; Strickley, R.; Wells, J.; Stuthman, K. S.; Van Tongeren, S. A.; Garza, N. L.; Donnelly, G.; Shurtleff, A. C.; Retterer, C. J.; Gharaibeh, D.; Zamani, R.; Kenny, T.; Eaton, B. P.; Grimes, E.; Welch, L. S.; Gomba, L.; Wilhelmsen, C. L.; Nichols, D. K.; Nuss, J. E.; Nagle, E. R.; Kugelman, J. R.; Palacios, G.; Doerffler, E.; Neville, S.; Carra, E.; Clarke, M. O.; Zhang, L. J.; Lew, W.; Ross, B.; Wang, Q.; Chun, K.; Wolfe, L.; Babusis, D.; Park, Y.; Stray, K. M.; Trancheva, I.; Feng, J. Y.; Barauskas, O.; Xu, Y. L.; Wong, P.; Braun, M. R.; Flint, M.; McMullan, L. K.; Chen, S. S.; Fearns, R.; Swaminathan, S.; Mayers, D. L.; Spiropoulou, C. F.; Lee, W. A.; Nichol, S. T.; Cihlar, T.; Bavari, S. Therapeutic efficacy of the small molecule GS-5734 against ebola virus in rhesus monkeys. *Nature* **2016**, *531*, 381−385.
(13) Amirian, E. S.; Levy, J. K. Current knowledge about the antivirals remdesivir (GS-5734) and GS-441524 as therapeutic options for coronaviruses. *One Health* **2020**, *9*, 100128.
(14) Williamson, B. N.; Feldmann, F.; Schwarz, B.; Meade-White, K.; Porter, D. P.; Schulz, J.; van Doremalen, N.; Leighton, I.; Yinda, C. K.; Pérez-Pérez, L.; Okumura, A.; Lovaglio, J.; Hanley, P. W.; Saturday, G.; Bosio, C. M.; Anzick, S.; Barbian, K.; Cihlar, T.; Martens, C.; Scott, D. P.; Munster, V. J.; de Wit, E. Clinical benefit of remdesivir in rhesus macaques infected with SARS-CoV-2. *Nature* **2020**, *585*, 273−276.
(15) Sun, D. Remdesivir for treatment of COVID-19: combination of pulmonary and iv administration may offer additional benefit. *AAPS J.* **2020**, *22*, 102.
(16) Mackman, R. L.; Hui, H. C.; Perron, M.; Murakami, E.; Palmiotti, C.; Lee, G.; Stray, K.; Zhang, L.; Goyal, B.; Chun, K.; Byun, D.; Siegel, D.; Simonovich, S.; Du Pont, V.; Pitts, J.; Babusis, D.; Vijjapurapu, A.; Lu, X.; Kim, C.; Zhao, X.; Chan, J.; Ma, B.; Lye, D.; Vandersteen, A.; Wortman, S.; Barrett, K. T.; Toteva, M.; Jordan, R.; Subramanian, R.; Bilello, J. P.; Cihlar, T. Prodrugs of a 1′-CN-4-aza-7, 9-dideazaadenosine C-nucleoside leading to the discovery of remdesivir (GS-5734) as a potent inhibitor of respiratory syncytial virus with efficacy in the African green monkey model of RSV. *J. Med. Chem.* **2021**, *64*, 5001−5017.
(17) Yan, V. C.; Muller, F. L. Why remdesivir failed: preclinical assumptions overestimate the clinical efficacy of remdesivir for COVID-19 and Ebola. *Antimicrob. Agents Chemother.* **2021**, *65*, No. e0111721.
(18) Malin, J. J.; Suarez, I.; Priesner, V.; Fatkenheuer, G.; Rybniker, J. Remdesivir against COVID-19 and other viral diseases. *Clin. Microbiol. Rev.* **2020**, *34*, No. e00162.
(19) Li, Y.; Cao, L.; Li, G.; Cong, F.; Li, Y.; Sun, J.; Luo, Y.; Chen, G.; Li, G.; Wang, P.; Xing, F.; Ji, Y.; Zhao, J.; Zhang, Y.; Guo, D.; Zhang, X. Remdesivir metabolite gs-441524 effectively inhibits SARS-CoV-2 infection in mouse models. *J. Med. Chem.* **2022**, *65*, 2785−2793.
(20) Zhang, L. L.; Zhou, R. H. Structural basis of the potential binding mechanism of remdesivir to SARS-CoV-2 RNA-dependent RNA polymerase. *J. Phys. Chem. B* **2020**, *124*, 6955−6962.
(21) Harrell, A. W.; Sychterz, C.; Ho, M. Y.; Weber, A.; Valko, K.; Negash, K. Interrogating the relationship between rat in vivo tissue distribution and drug property data for > 200 structurally unrelated molecules. *Pharmacol. Res. Perspect.* **2015**, *3*, No. e00173.
(22) Toelzer, C.; Gupta, K.; Yadav, S. K. N.; Borucu, U.; Davidson, A. D.; Kavanagh Williamson, M. K.; Shoemark, D. K.; Garzoni, F.; Staufer, O.; Milligan, R.; Capin, J.; Mulholland, A. J.; Spatz, J.; Fitzgerald, D.; Berger, I.; Schaffitzel, C. Free fatty acid binding pocket in the locked structure of SARS-CoV-2 spike protein. *Science* **2020**, *370*, 725−730.
(23) Sun, D.; Gao, W.; Hu, H.; Zhou, S. Why 90% of clinical drug development fails and how to improve it? *Acta Pharm. Sin. B* **2022**, *12*, 3049−3062 in press.
(24) Gao, W.; Hu, H.; Dai, L.; He, M.; Yuan, H.; Zhang, H.; Liao, J.; Wen, B.; Li, Y.; Palmisano, M.; Traore, M. D. M.; Zhou, S.; Sun, D. Structure−tissue exposure/selectivity relationship (STR) correlates with clinical efficacy/safety. *Acta Pharm. Sin. B* **2022**, *12*, 2462−2478 in press.
(25) Ramakrishnan, M. A. Determination of 50% endpoint titer using a simple formula. *World J. Virol.* **2016**, *5*, 85−86.
(26) Siegel, D.; Hui, H. C.; Doerffler, E.; Clarke, M. O.; Chun, K.; Zhang, L.; Neville, S.; Carra, E.; Lew, W.; Ross, B.; Wang, Q.; Wolfe, L.; Jordan, R.; Soloveva, V.; Knox, J.; Perry, J.; Perron, M.; Stray, K. M.; Barauskas, O.; Feng, J. Y.; Xu, Y. L.; Lee, G.; Rheingold, A. L.; Ray, A. S.; Bannister, R.; Strickley, R.; Swaminathan, S.; Lee, W. A.; Bavari, S.; Cihlar, T.; Lo, M. K.; Warren, T. K.; Mackman, R. L. Discovery and synthesis of a phosphoramidate prodrug of a pyrrolo(2,1-f][triazin-4-amino] adenine C-nucleoside (GS-5734) for the treatment of Ebola and emerging viruses. *J. Med. Chem.* **2017**, *60*, 1648−1661.
(27) Slusarczyk, M.; Lopez, M. H.; Balzarini, J.; Mason, M.; Jiang, W. G.; Blagden, S.; Thompson, E.; Ghazaly, E.; McGuigan, C. Application of ProTide technology to gemcitabine: a successful approach to overcome the key cancer resistance mechanisms leads to a new agent (NUC-1031) in clinical development. *J. Med. Chem.* **2014**, *57*, 1531−1542.
(28) Kneller, D. W.; Li, H.; Galanie, S.; Phillips, G.; Labbé, A.; Weiss, K. L.; Zhang, Q.; Arnould, M. A.; Clyde, A.; Ma, H.; Ramanathan, A.; Jonsson, C. B.; Head, M. S.; Coates, L.; Louis, J. M.; Bonnesen, P. V.; Kovalevsky, A. Structural, electronic, and electrostatic determinants for inhibitor binding to subsites S1 and S2 in SARS-CoV-2 main protease. *J. Med. Chem.* **2021**, *64*, 17366−17383.
(29) Banerjee, S.; Yadav, S.; Banerjee, S.; Fakayode, S. O.; Parvathareddy, J.; Reichard, W.; Surendranathan, S.; Mahmud, F.; Whatcott, R.; Thammathong, J.; Meibohm, B.; Miller, D. D.; Jonsson, C. B.; Dubey, K. D. Drug repurposing to identify nilotinib as a potential SARS-CoV-2 main protease inhibitor: insights from a computational and in vitro study. *J. Chem. Inf. Model.* **2021**, *61*, 5469−5483.
(30) Kneller, D. W.; Li, H.; Phillips, G.; Weiss, K. L.; Zhang, Q.; Arnould, M. A.; Jonsson, C. B.; Surendranathan, S.; Parvathareddy, J.; Blakeley, M. P.; Coates, L.; Louis, JM; Bonnesen, PV; Kovalevsky, A. Covalent narlaprevir-and boceprevir-derived hybrid inhibitors of SARS-CoV-2 main protease. *Nat. Commun.* **2022**, *13*, 2268−11.
(31) Bocci, G.; Bradfute, S. B.; Ye, C.; Garcia, M. J.; Parvathareddy, J.; Reichard, W.; Surendranathan, S.; Bansal, S.; Bologa, C. G.; Perkins, D. J.; Jonsson, C. B.; Sklar, L. A.; Oprea, T. I. Virtual and in vitro antiviral screening revive therapeutic drugs for COVID-19. *ACS Pharmacol. Transl. Sci.* **2020**, *3*, 1278−1292.
(32) Severson, W. E.; Shindo, N.; Sosa, M.; Fletcher, T., III; White, E. L.; Ananthan, S.; Jonsson, C. B. Development and validation of a high-throughput screen for inhibitors of SARS CoV and its application in screening of a 100,000-compound library. *J. Biomol. Screen* **2007**, *12*, 33−40.

https://doi.org/10.1021/acs.jmedchem.2c00758
J. Med. Chem. XXXX, XXX, XXX−XXX